Research Square

Preprints are preliminary reports that have not undergone peer review.
They should not be considered conclusive, used to inform clinical practice,
or referenced by the media as validated information.

Frictional instability in dry quartz gouge from room to elevated temperatures

Shoya Uchikoshi

5193066907@g.ecc.u-tokyo.ac.jp

The University of Tokyo

Hiroshi Sakuma

National Institute for Materials Science

Ikuo Katayama

Kyoto University

Kenji Kawai

The University of Tokyo

Research Article

Keywords: Quartz, Unstable slip, Dry condition, Temperature dependence

Posted Date: November 18th, 2026

DOI: https://doi.org/10.21203/rs.3.rs-11562621/v1

License: This work is licensed under a Creative Commons Attribution 4.0 International License.
Read Full License

Additional Declarations: No competing interests reported.

Article

Frictional instability in dry quartz gouge from room to elevated temperatures

Shoya Uchikoshi [a, b,*], Hiroshi Sakuma [b], Ikuo Katayama[c], and Kenji Kawai [a]

[a] Department of Earth and Planetary Science, The University of Tokyo, Tokyo, Japan

[b] National Institute for Materials Science, Ibaraki, Japan

[c] Department of Earth and Planetary Sciences, Graduate School of Science, Kyoto University, Kyoto, Japan

* Correspondence: 5193066907@g.ecc.u-tokyo.ac.jp

Abstract: The frictional properties of fault materials exert a strong influence on fault dynamics and earthquake generation. The velocity dependence of friction, a key factor controlling slip instability, can be modified by temperature, pressure, and the presence of water. Understanding of the frictional properties of dry quartz gouge is necessary to evaluate the effect of water. To investigate the slip stability of dry quartz gouge, velocity-step shear experiments were performed using a double-direct shear apparatus at a normal stress of 10 MPa, temperatures from 30 °C to 400 °C, and sliding velocities from 0.36 μm/s to 39 μm/s. The steady-state friction coefficients at 3.0 μm/s ranged from 0.619 to 0.712 and showed little temperature dependence. Immediate frictional responses were observed following changes in sliding velocity, and the steady-state friction coefficients decreased with increasing velocity. The velocity-dependent frictional behavior was analyzed within the framework of rate-and-state friction (RSF) theory. The a parameter (direct effect) exhibited a weakly negative or negligible temperature dependence, whereas the b parameter (evolution effect) increased slightly with increasing temperature. As a result, the $a - b$ values were negative at all tested temperatures and became increasingly negative with increasing temperature. These results indicate that frictional instability can occur in dry quartz gouge even in the absence of water.

Keywords: Quartz; Unstable slip; Dry condition; Temperature dependence

Acknowledgments: We gratefully acknowledge the work of past and present members of our laboratory. We also thank Keishi Okazaki for experiments. This work was supported by Japan Society for the Promotion of Science KAKENHI Grant 24K00795 to HS, 24K07171 and 23K25970 to KK, and 23H00152 to IK.

1. Introduction

Earthquakes often occur through the movement of pre-existing faults, and the frictional behavior of gouges in faults is critical to fault dynamics. The frictional properties of quartz, one of the most common minerals in natural faults, have been studied mainly through laboratory experiments under various conditions by controlling the confining pressure, pore pressure, temperature, humidity, and sliding velocity. However, the temperature dependence of velocity-dependent frictional behavior in quartz gouge remains controversial, particularly under dry and conditions (Morrow et al. 2000; Masuda et al. 2019; Chester and Higgs 1992). Understanding this temperature dependence is essential for evaluating the fault slip stability and distinguishing the effects of temperature from those of water.

The frictional stability is often evaluated based on the rate and state friction (RSF) framework (Dieterich 1979; Ruina 1983). In this framework, the friction coefficient μ at the slip velocity V of a gouge is described as follows:

$$\mu = \mu_0 + a \ln\left(\frac{V}{V_0}\right) + b \ln\left(\frac{V_0\theta}{D_c}\right) \quad (1)$$

Here, μ_0 is the steady-state friction coefficient at a reference slip rate V_0, a is a parameter that represents the direct effect, b is a parameter that represents the evolution effects, θ is a state variable, and D_c is the characteristic slip distance. The time evolution of the state valuable θ is described as the slip law (Ruina 1983):

$$\frac{d\theta}{dt} = -\frac{V\theta}{D_c} \ln\left(\frac{V\theta}{D_c}\right), \quad (2)$$

or the aging law (e.g. Dieterich 1979):

$$\frac{d\theta}{dt} = 1 - \frac{V\theta}{D_c}. \quad (3)$$

Eq. (2) (slip law) was used in this study because the slip law can fit the experimental results better than the aging law (Bhattacharya et al. 2015). In these equations, the value of $a - b$ is essential for understanding the stability of the slip. A negative $a - b$ value accelerates the slip by increasing the slip rate, which can cause unstable slip (Scholz 1998). A positive $a - b$ decelerates slip with increasing slip rate and stabilizes the slip.

For quartz gouge, the $a - b$ values at temperatures from room to 600 °C and the effective confining pressure of 150 MPa were reported to be positive at dry conditions and the slip velocities of 0.5-5.0 μm/s (Masuda et al. 2019). On the contrary, stick-slip behavior, which implies the unstable slip of the gouge, was reported for dry quartz gouge at room temperature, normal stress of 100 MPa, and slip velocity of 0.5 μm/s (Morrow et al. 2000). Negative $a - b$ of dry quartz gouge was reported at elevated temperatures of 300 and 450 °C and confining pressure of 150 MPa by the slide-hold-slide (SHS) tests (Chester and Higgs 1992).

However, these experiments were conducted under limited conditions, especially at high confining pressures. Therefore, systematic experiments at low confining pressures with

varying temperatures are required to reveal the frictional stability of dry quartz gouge in the crust. Another advantage of conducting shear experiments at low confining pressures is that the influence of water on friction is minimized because high confining pressure opens the pathway to absorb moisture (Dieterich and Conrad 1984).

Hence, this study conducted velocity-step experiments using the double-direct shear apparatus to ascertain the constitutive parameters of dry quartz gouge from room temperature to 400 °C at a low normal stress of 10 MPa with long shear displacement. We then discussed the effect of temperature to better understand the frictional stability conditions of dry quartz gouge.

2. Methods

2.1. Sample characteristics

Quartz particles separated from a granite rock were used as a simulated fault gouge without further purification. X-ray diffraction analysis (Ultima IV, Rigaku) revealed that quartz is the major component with traces of feldspar (SI Fig. 1 and Table S2). The mineral composition of quartz was estimated to be 88.5 wt.% (SI Tables 1 and 2) from the chemical analysis by inductively coupled plasma optical emission spectrometer (Agilent 5800 ICP-OES). Particle diameters measured by a laser particle diameter analyzer (SALD-7100, Shimadzu Corp.) range from 0.2 to 60 μm, as plotted in SI Fig. 2. The median and average values are 5.968 μm and 9.454 μm, respectively.

2.2. Double-direct shear tests

The double-direct shear testing machine (Noda and Shimamoto 2009) at Hiroshima University in Japan was used for velocity-step friction tests. The quartz particles were dried in a vacuum oven at 100 °C for 19 hours before shear experiments. There are two gouge layers in the testing machine, one on each side of the center block as shown in Fig. 1. The thickness of each gouge layer formed by 2 g of quartz particles was approximately 0.5 mm, embedded between two blocks with an area of 50 × 40 mm. The surfaces of these blocks

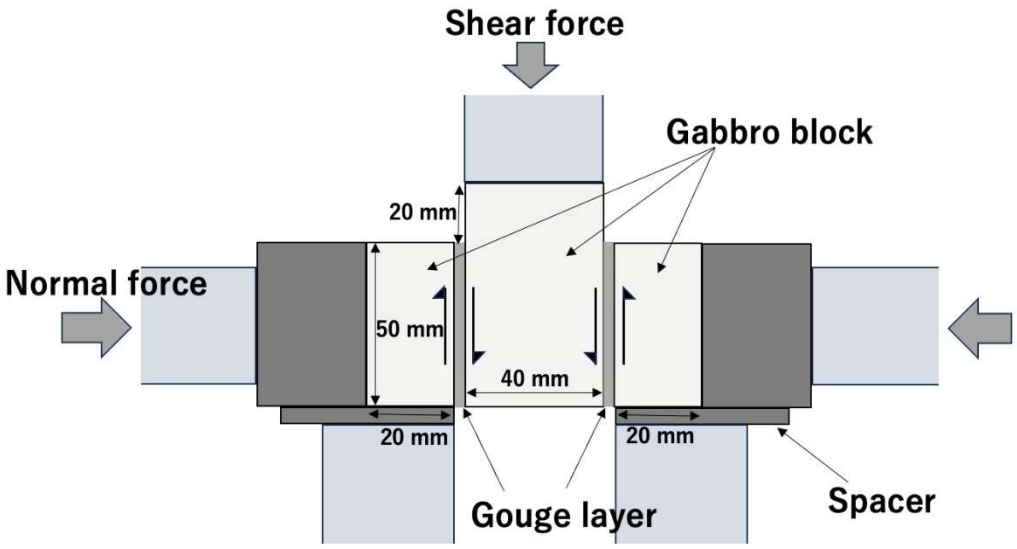


Fig. 1 The sample assembly for the frictional experiments performed by double-direct shear apparatus at Hiroshima University (Noda and Shimamoto 2009). The width of gabbro block is 40 mm.

were polished with silicon carbide abrasive (Japanese Industrial Standard #80, with a particle size range of approximately 180-212 μm). Before the shear experiments, a normal stress of 10 MPa was applied for 1 hour as precompaction. The sample temperature was controlled following the method of Kubo and Katayama (2015). Briefly, gabbro blocks and samples were placed in a heater frame. They were heated by external furnaces mounted in the heater frame up to 400 °C, with the temperature monitored by thermocouples located near the center of the sample assembly. The shear experiments were performed with a constant normal stress of 10 MPa and temperatures at 30, 100, 200, 300, and 400 °C. During the tests, shear displacement, shear stress and normal stress were continuously measured with a data sampling frequency of 100 Hz.

The velocity-step tests were initiated after 5 mm of shear displacement (Fig. 2). The load-point velocity was first increased from 3.0 to 39 μm/s as the first velocity step. After 1.0 mm of shear displacement, the velocity was decreased back to 3.0 μm/s as the second velocity step. This sequence was repeated twice, resulting in a velocity-stepping pattern of 3.0→39→3.0→39→3.0 μm/s. Similar tests were conducted for velocity changes between 3.0 and 0.36 μm/s following the sequence 3.0→0.36→3.0→0.36 μm/s.

2.3. Estimation of rate-and-state friction parameters

From the measured normal stress σ and shear stress τ, the friction coefficient is calculated by

$$\mu = \tau/\sigma. \quad (4)$$

All analysis to determine the RSF parameters was conducted using the RSFit3000 program (Skarbek and Savage 2019). First, the detrending procedure was conducted on the friction coefficient before the velocity step. Then, a, b, D_c, and system stiffness k were determined by fitting the data to Eqs. (1) and (2) using a non-linear least-squares method.

3. Results

3.1. Evolution of frictional strength

For all investigated temperatures, the friction coefficient increased with shear displacement, reaching a maximum between 1 and 3 mm, and then decreased to the steady-state friction coefficient at around 4-6 mm (Fig. 2). No clear difference in the curves was observed between 30 and 100 °C, whereas a large decrease in the friction coefficient with increasing displacement after the maximum was observed at higher temperatures from 200 to 400 °C. The maximum friction coefficient (μ_{max}) and the steady-state friction coefficient (μ_{ss}) at each temperature are listed in Table 1. Here, μ_{ss} is defined as the friction coefficient measured during 3.0 mm of shear displacement after μ_{max} is reached. At 30 °C, μ_{max} was 0.690, and μ_{ss} decreased slightly to 0.683. At 400 °C, μ_{max} and μ_{ss} were 0.687 and 0.645, respectively. The decrease in friction coefficient ($\mu_{max} - \mu_{ss} = 0.042$) was larger than at other temperatures (Fig. 2, Table 1).

Table 1 Temperature, friction coefficient, and constitutive parameters on dry quartz powders

Run ID	T [°C]	μ_{max}	μ_{ss}[a]	$\mu_{max} - \mu_{ss}$	a[b]	b[b]	$a - b$[b]	D_c [μm]
HTB0818	30	0.690	0.683	0.007	0.0098 ± 0.0017	0.0107 ± 0.0017	-0.0009 ± 0.0003	2.97 ± 1.32
HTB0821	100	0.677	0.669	0.008	0.0086 ± 0.0017	0.0097 ± 0.0017	-0.0012 ± 0.0003	3.18 ± 0.87
HTB0819	200	0.707	0.692	0.015	0.0089 ± 0.0017	0.0107 ± 0.0020	-0.0018 ± 0.0004	3.30 ± 0.90
HTB0822	300	0.712	0.674	0.038	0.0099 ± 0.0020	0.0115 ± 0.0021	-0.0016 ± 0.0007	3.22 ± 0.82
HTB0820	400	0.687	0.645	0.042	0.0070 ± 0.0008	0.0098 ± 0.0007	-0.0027 ± 0.0001	4.75 ± 1.02

[a] Friction coefficient at 3.0 mm of shear displacement relative to the maximum friction coefficient.

130 [b] Constitutive parameters a, b, $a - b$, D_c averaged over all steps with the error of standard deviation.

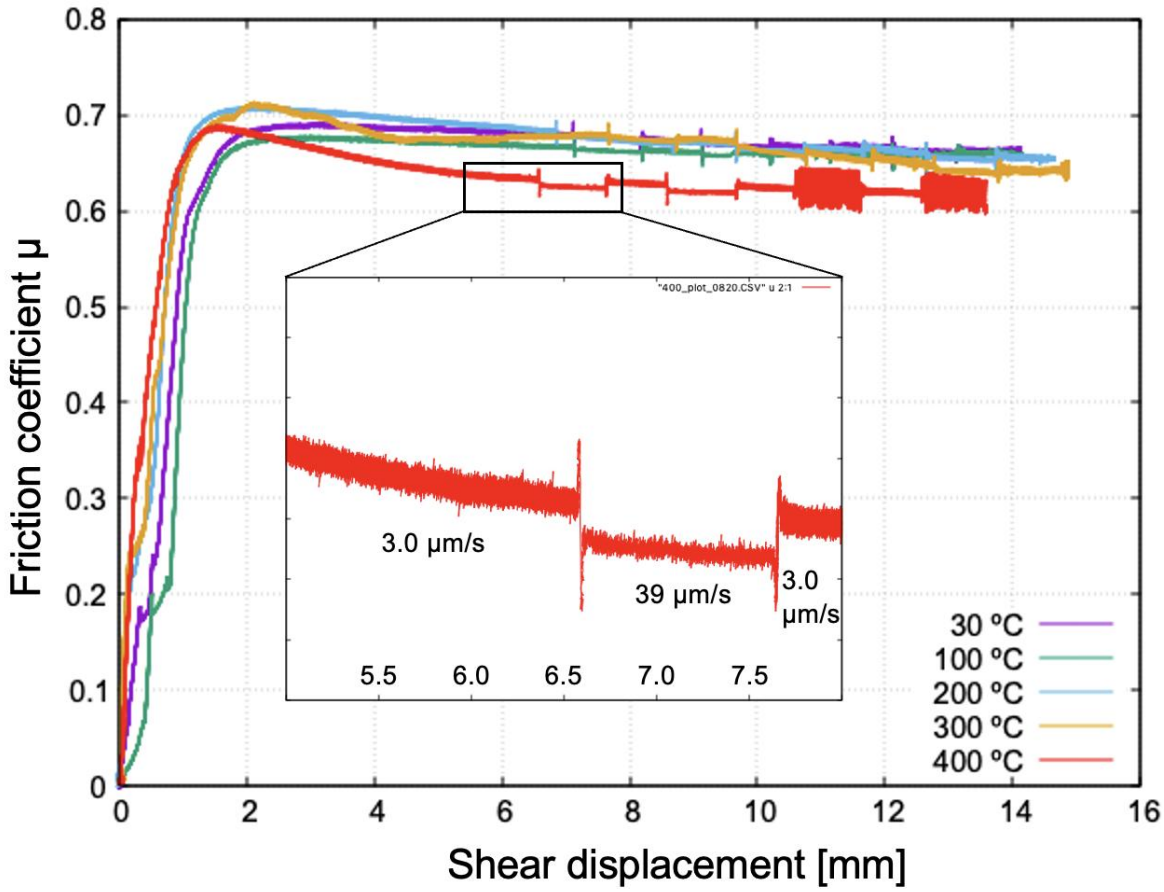


Fig. 2 Friction coefficient as a function of shear displacement for each temperature. The load-point velocity is 3.0 μm/s before first velocity-step. The black square shows enlarged view of velocity-step. Each curve includes 3 up steps and 4 down steps.

131 *3.2. Velocity-step tests and RSF parameters*

Some typical behaviors of friction coefficients during the velocity-step tests were plotted in Fig. 3. The immediate increase in friction coefficient after the increase in velocity and a subsequent damped oscillation were observed at the up-step test (Fig. 3b). This oscillation is similar to a state near the onset of unstable sliding, where stick-slip can occur (Leeman et al. 2018). The steady-state friction coefficient decreased after the velocity increased. Stick-slip behavior was observed only at 400 °C and at the lowest velocity of 0.36 μm/s, as shown in Figs. 2 and 4.

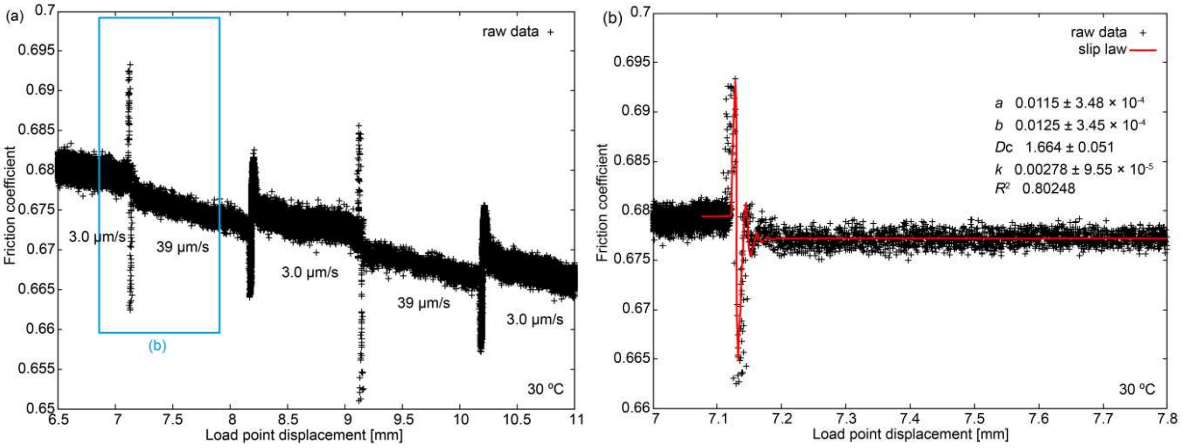


Fig. 3 Enlarged view of friction coefficient versus load-point displacement curve at 30 °C. (a) Raw data of velocity-step tests from 3.0 to 39 μm/s and from 39 to 3.0 μm/s. (b) Enlarged view of the fitting result for the velocity step from 3.0 to 39 μm/s. The red line indicates the fitted curve.

The $a - b$ values obtained by fitting the RSF model to all velocity-step tests, except those conducted at 400 °C and 0.36 μm/s, are plotted as a function of temperature in Fig. 5. The $a - b$ values were negative at all temperatures and decreased with increasing temperatures (Fig. 5 and Table 1). The $a - b$ values obtained from the up-step and down-step procedures show no clear difference.

The a parameters obtained from each velocity-step test are plotted in Fig. 6. The values obtained from up-step tests were higher than those from down-step tests for almost all temperatures. Overall, the a values appear to decrease slightly with increasing temperature (Fig. 6 and Table 1). Although the data exhibit some scatter, the a values tended to be larger

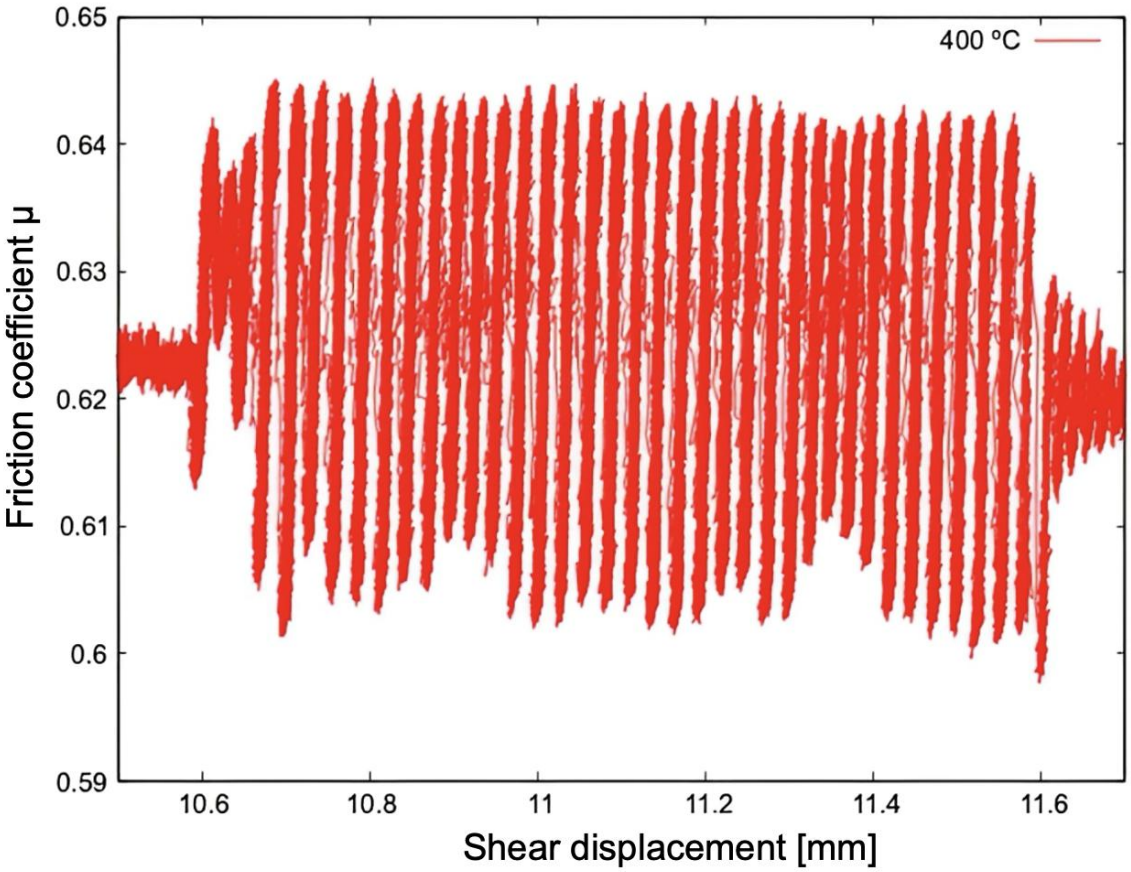


Fig. 4 Stick-slips observed in friction coefficients as a function of shear displacement at 400 °C with a velocity of 0.36 μm/s.

148 for velocity steps at lower velocities (0.36 μm/s ↔ 3.0 μm/s) than for those at higher
149 velocities (3.0 μm/s ↔ 39 μm/s).

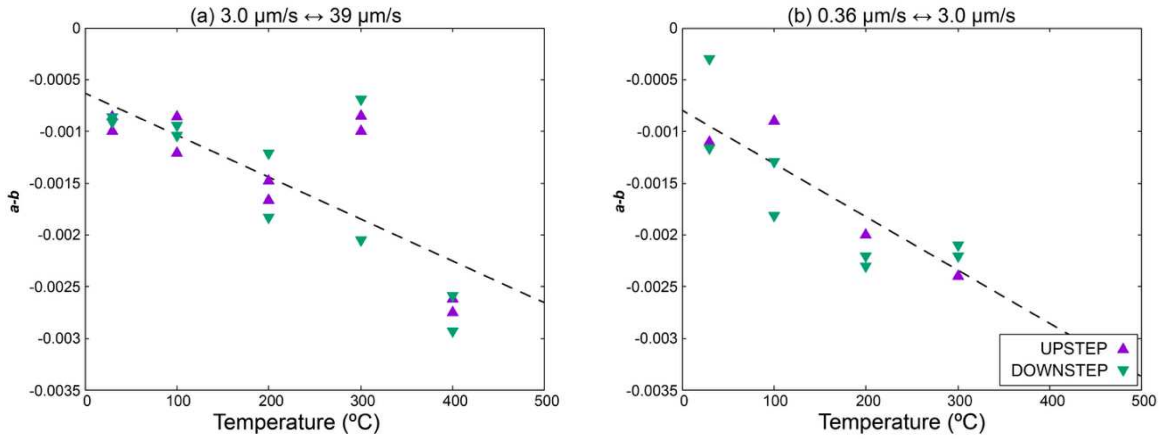


Fig. 5 The $a - b$ values plotted as a function of temperature. (a) $a - b$ values obtained from velocity-step tests between 3.0 and 39 μm/s. (b) $a - b$ values obtained from velocity-step tests between 0.36 and 3.0 μm/s. The dashed lines represent least-squares fits to straight lines.

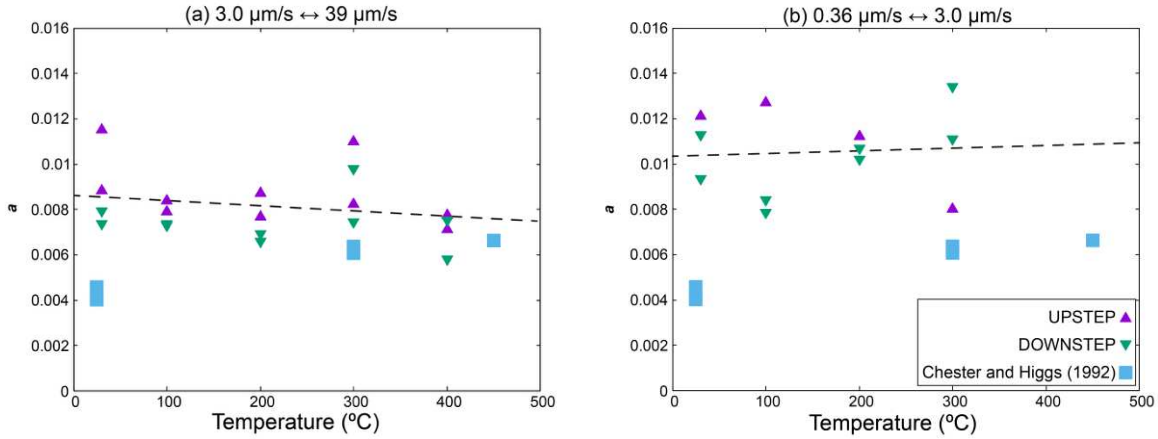


Fig. 6 Temperature dependence of the a value. (a) a values obtained from velocity-step tests between 3.0 and 39 μm/s. (b) a values obtained from velocity-step tests between 0.36 and 3.0 μm/s. Light blue squares indicate a values obtained from slide-hold-slide tests performed using a triaxial machine on quartz gouge with particle diameters of less than 100 μm (Chester and Higgs 1992). The dashed lines represent least-squares fits to straight lines.

As shown in Fig. 7, the b parameters obtained from up-step tests were generally higher than those from down-step tests. In addition, the b values increased slightly with temperature for all velocity steps. (Fig. 7 and Table 1).

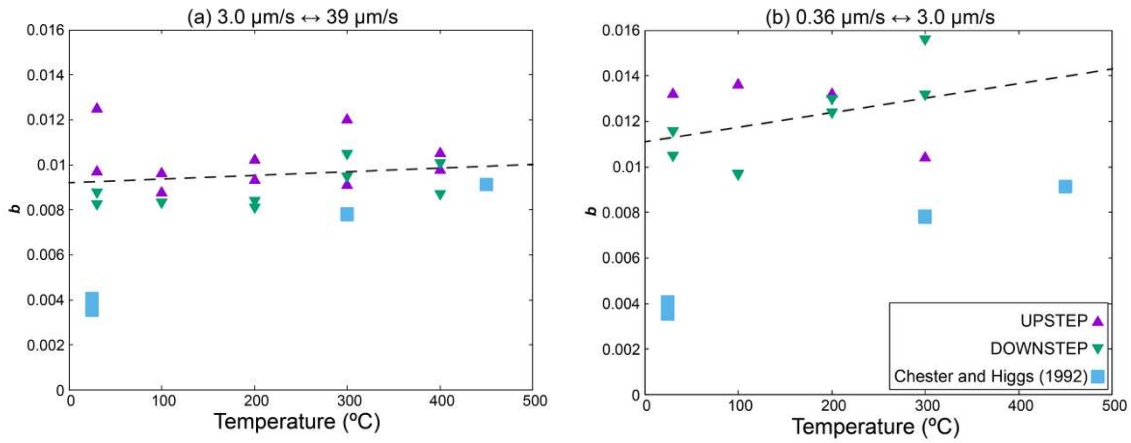


Fig. 7 Temperature dependence of the b values. (a) b values obtained from velocity-step tests between 3.0 and 39 μm/s. (b) b values obtained from velocity-step tests between 0.36 and 3.0 μm/s. Light blue squares indicate b values obtained from slide-hold-slide tests performed using a triaxial machine on quartz gouge with particle diameters of less than 100 μm (Chester and Higgs 1992). The dashed lines represent least-squares fits to straight lines.

153 The D_c values obtained from velocity steps at lower velocities (0.36 μm/s ↔ 3.0 μm/s)
154 were smaller than those obtained from velocity steps at higher velocities (3.0 μm/s ↔ 39
155 μm/s) (Fig. 8). The D_c values appeared to increase with increasing temperature for the up-
156 step tests, whereas the opposite trend was observed for the down-step tests.

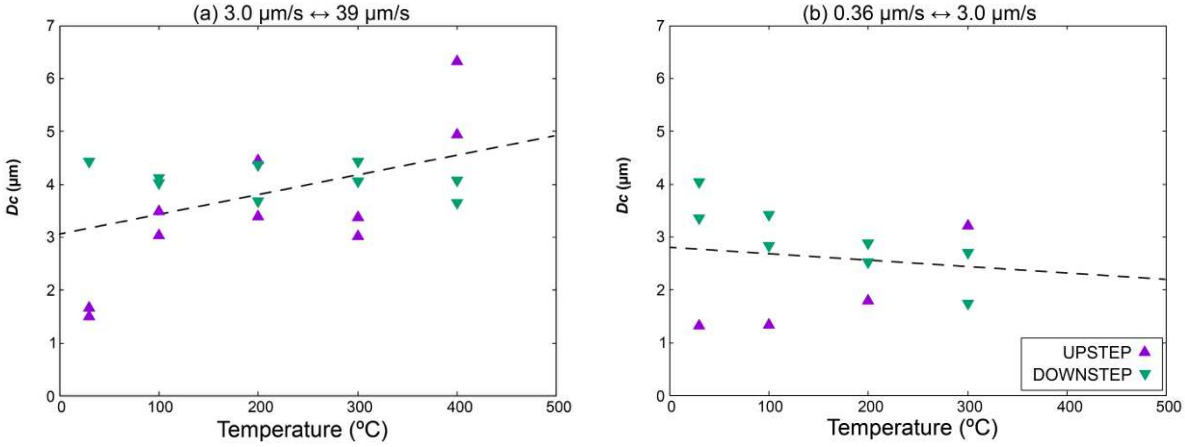


Fig. 8 Temperature dependence of the critical slip distance (D_c). (a) D_c values obtained from velocity-step tests between 3.0 and 39 μm/s. (b) D_c values obtained from velocity-step tests between 0.36 and 3.0 μm/s. The dashed lines represent least-squares fits to straight lines.

157 **4. Discussion**

4.1. Strain-weakening behavior at elevated temperatures

The $\mu_{max} - \mu_{ss}$ values represent the magnitude of strain weakening. Significant strain weakening results from shear localization and the associated development of boundary-parallel shear (e.g., Marone 1998; Niemeijer et al. 2010). In this study, the $\mu_{max} - \mu_{ss}$ values increased with temperature. This trend in $\mu_{max} - \mu_{ss}$ may reflect the progressive development of boundary-parallel shear with increasing temperature. As expected, the microstructures observed in this study exhibited both Riedel shear and boundary-parallel shear at 30 °C, whereas the recovered sample at 200 °C was showed only by boundary-parallel shear (SI Fig. 3). However, no localized shear structures were observed at 400 °C. Therefore, the large magnitude of strain weakening at 400 °C may not be attributable to the development of boundary-parallel shear. Instead, the decrease in $\mu_{max} - \mu_{ss}$ values at 400 °C may reflect a reduction in yield strength associated with ductile rather than brittle deformation. In this temperature range, the difference of deformation mechanisms may control the temperature dependent friction coefficient change.

4.2. Frictional stability of dry quartz gouge and physics behind the RSF parameters

The negative $a - b$ values imply that unstable slip can occur in dry quartz gouge under the tested conditions. This result contrasts with the common understanding that the presence of water is essential for unstable slip in quartz gouge (e.g., Masuda et al. 2019). This discrepancy may reflect differences in confining pressure. Although the physical origin of the negative $a - b$ values observed at the low normal stress of 10 MPa is not yet fully understood, we attempt to interpret this behavior within the framework of traditional rate-and-state friction theory.

The decrease in the $a - b$ value with increasing temperature is due to slight changes in a and b (Figs. 6, 7, and 9). The a value is generally interpreted to be associated with thermally activated creep at contact junctions (Nakatani 2001; Rice et al. 2001; Liu and He 2023). In this hypothesis, the slip velocity is described by the Arrhenius equation:

$$V = V_0 \exp\left(-\frac{Q - \tau_c \Omega}{kT}\right), \tag{5}$$

where Q is activation energy, τ_c is shear stress at contact junctions, Ω is activation volume, k is the Boltzmann constant, and T is the absolute temperature (Heslot et al. 1994; Sleep 1997; Nakatani 2001). From Eqs. (4) and (5), the friction coefficient μ is described as

$$\mu = \frac{Q}{\Omega \sigma_c} + \frac{kT}{\Omega \sigma_c} \ln\left(\frac{V}{V_0}\right), \tag{6}$$

where σ_c is the normal stress at contact junctions. Comparing Eqs. (1) and (6), a is described as follows:

$$a = \frac{kT}{\Omega\sigma_c}, \tag{7}$$

suggesting that a linearly increases with T, when Ω and τ_c are constant. However, this relationship was not observed for dry quartz gouge in this study. Such negative or neutral temperature dependence at temperatures below 350 °C was also reported for various species of minerals and rocks (Barbot 2024). Therefore, the thermally activated theory may not be applied for low-temperature conditions. The mechanism underlying the negative or neutral temperature dependence of the a value may be related to dislocation motion within quartz particles. For example, a decrease in the a value with increasing temperatures from 22 to 200 °C was observed for friction between single-crystal muscovite (001) surfaces, and this behavior was attributed to a reduction in dislocation density (Sakuma et al. 2026). If dislocation mobility influences the a value for quartz gouge, the negative or neutral temperature dependence may be associated with the limited mobility of dislocations at temperatures below 300 °C, where dislocation glide kinetics are relatively slow (Lloyd and Knipe 1992).

The b value is generally believed to be associated with the healing phenomenon at the real contact area (e.g., Marone 1998). Temperature dependence of the parameter b can be derived from the Brechet and Estrin (BE) model (Brechet and Estrin 1994) for logarithmic time-dependent healing and an Arrhenius-type relation (Nakatani and Scholz 2004) as follows:

$$b = \frac{\mu_0 RT}{\Omega\sigma_0}, \tag{8}$$

where $\sigma_0 \equiv \sigma\,(t = 0)$, σ is the normal contact stress, t is quasi-stationary contact time, and R is the gas constant. The b value exhibited clear temperature sensitivity in wet experiments (Chester and Higgs 1992). Because the healing rates of quartz gouges are similar under dry and wet conditions (Katayama et al. 2015), the b value may also increase with increasing temperature under dry conditions, consistent with our results.

4.3. Implications of the Comparison with previous studies

The experimental conditions of this study and previous experiments on quartz powders (Chester and Higgs 1992; Morrow et al. 2000; Masuda et al. 2019) are summarized in Table 2. Our $a - b$ values obtained under dry conditions (Fig. 9a and Table 2) are similar to those reported from SHS tests by Chester and Higgs (1992). Furthermore, the negative $a - b$ values are consistent with the occurrence of stick-slip behavior observed in dry quartz gouge at a confining pressure of 100 MPa and room temperature (Morrow et al. 2000).

In the SHS test, the load-point velocity is reduced to zero for a specified hold period and then restored to its original value to evaluate the time-dependent recovery of frictional strength. However, owing to the finite stiffness of the testing machine, the slip velocity of the sample does not become completely zero during the hold period. Consequently, the $a - b$

values obtained from SHS tests represent frictional behavior at the lowest sliding velocities among these experiments.

The similarity between the $a - b$ values from our velocity-step tests and those from SHS tests suggests that $a - b$ values are relatively insensitive to slip velocity over the range from near-zero slip rates to the velocities applied in the present study.

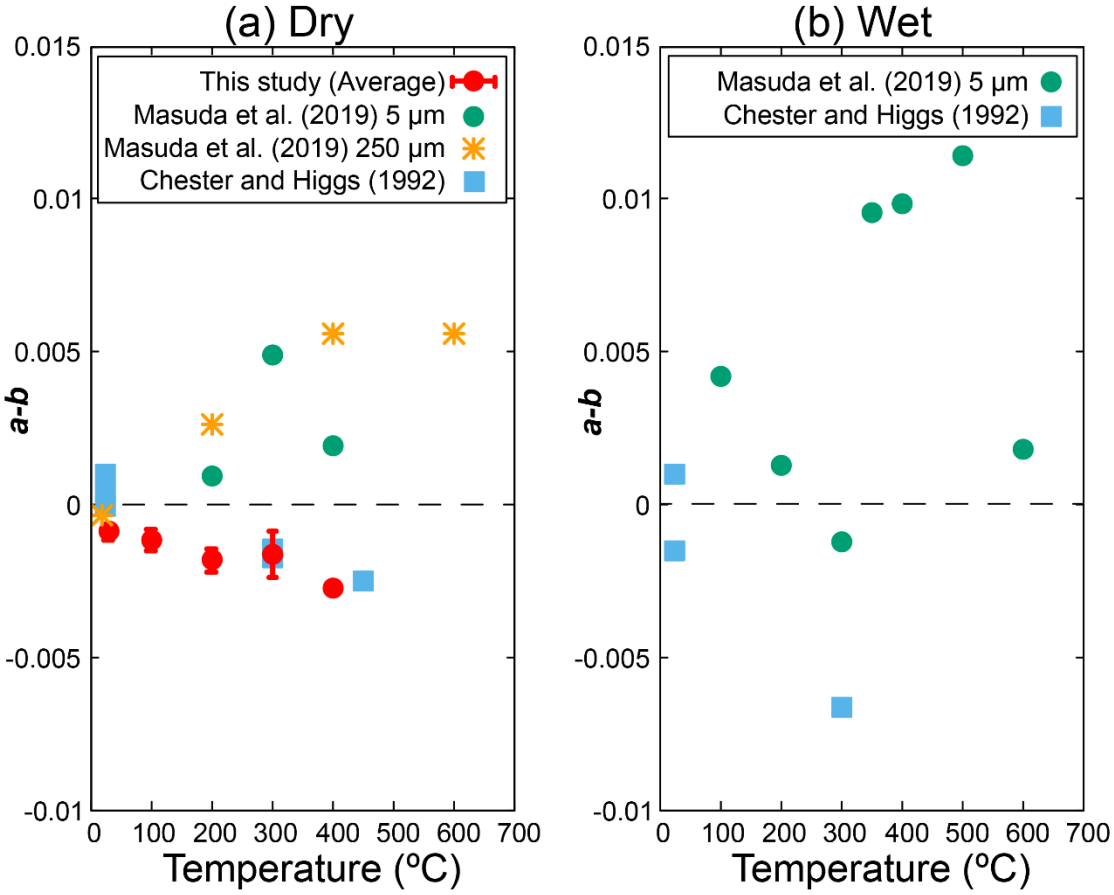


Fig. 9 Temperature dependence of the $a - b$ values. (a) $a - b$ values obtained under dry conditions. Light blue squares indicate $a - b$ values obtained from slide-hold-slide tests performed using a triaxial machine on quartz gouge with particle diameters of less than 100 μm (Chester and Higgs 1992). Green circles and yellow asterisks indicate $a - b$ values from velocity-step tests performed using a triaxial machine on quartz gouge with particle diameters of 5 and 250 μm, respectively (Masuda et al. 2019). (b) $a - b$ values obtained under wet conditions. Green circles represent data from Masuda et al. (2019), whereas light blue squares represent data from Chester and Higgs (1992).

In contrast, positive $a - b$ values and an increase in these values with increasing temperature were reported by Masuda et al. (2019). The normal stress applied in the experiments of Masuda et al. (2019) and Chester and Higgs (1992) was the same (150 MPa). Therefore, the discrepancy between our results obtained at 10 MPa and those of Masuda et al. (2019) cannot be explained solely by the differences in normal stress, because our results are consistent with those of Chester and Higgs (1992).

The average particle diameters used by Masuda et al. (2019) were 5 and 250 μm, representing the smallest and largest particle sizes among the studies considered here. Bedford and Faulkner (2021) showed that larger particle sizes promote stable slip in quartz gouge under wet conditions, although the effect of particle size on slip stability under dry conditions has not yet been investigated. If the trend observed under wet conditions also applies under dry conditions, a difference in the $a - b$ values would be expected between the 5 and 250 μm samples. However, no clear difference was observed.

Even a small amount of water can influence frictional behavior. Under wet conditions, the $a - b$ values decreased with increasing temperature up to 300 °C (Fig. 9b) and became negative at 300 °C. Masuda et al. (2019) and Chester and Higgs (1992) did not report details of the drying procedures used in their experiments, leaving the role of water uncertain. In contrast, the samples used by Morrow et al. (2000) were dried at 180 °C for several days, which would have substantially reduced the influence of water. Stick-slip was observed in their experiments, indicating that dry quartz gouge can exhibit negative $a - b$ values even in the absence of water at room temperature. This observation is consistent with our results and supports the interpretation that the drying procedure used in the present study effectively minimized the influence of water.

Table 2 Comparison of experimental conditions for quartz powders

Condition	**This study**	**Masuda et al. (2019)[a]**	**Masuda et al. (2019)[a]**	**Chester and Higgs (1992)**	**Chester and Higgs (1992)**	**Morrow et al. (2000)[b]**
$a - b$	**negative**	**positive**	**negative**	**negative**	**negative**	**N/A (stick-slip)**
Dry or Wet	dry	dry	wet	dry	wet	dry
Effective normal stress [MPa]	10	150	150	150	150	100
Particle diameter [μm]	< 60	5 or 250	5	< 100	< 100	< 90
Drying time	19 h	unknown	unknown	unknown	unknown	Several days
Drying temperature [°C]	100	unknown	unknown	unknown	unknown	180

[a] Particle diameter in Masuda et al. (2019) is the average.

[b] The $a - b$ values were not available in Morrow et al. (2000).

Although the reason for the difference in $a - b$ values among dry quartz gouge experiments remains unresolved, the present comparison suggests that no single experimental parameter can adequately explain the observed variability. Instead, $a - b$ values are likely controlled by the combined effects of multiple factors, including normal stress, sliding velocity, and a small amount of water. The results of this study provide new constraints on the frictional behavior of dry quartz gouge at low normal stress, demonstrating that quartz gouge can promote unstable slip even under dry conditions. These findings provide a new perspective on the origin of unstable slip in quartz-rich fault materials and highlight the need for systematic experiments over a broader range of conditions.

5. Conclusions

In this study, we investigated the frictional behavior of dry quartz gouge, one of the most abundant minerals in the Earth's crust. Velocity-step shear experiments were conducted to determine the rate-and-state friction (RSF) parameters at temperatures ranging from room temperature to 400 °C. The $a - b$ values were negative in all experiments, and their average values decreased with increasing temperature. Although the a value exhibited a weakly negative or negligible temperature dependence, the b value increased slightly with temperature. The temperature-dependent decrease in $a - b$ value is therefore primarily attributed to the increase in the b parameters. The physical and chemical mechanisms responsible for the temperature dependence of the a parameter cannot be fully explained by conventional thermal activation theory.

The occurrence of frictional instability observed as stick-slip behavior, together with increasingly negative $a - b$ values at elevated temperatures, demonstrates that dry quartz gouge can promote unstable slip over a wide temperature range. These findings provide new constraints on the frictional behavior of dry quartz gouge under low normal-stress conditions and suggest that dry quartz gouge can promote unstable slip even in the absence of water. This study highlights the importance of considering dry frictional processes in fault mechanics and provides a foundation for future investigations into the factors controlling slip stability in the crust.

Appendix A. Supplementary data

Supplementary data to this article can be found online at …

Funding: This work was supported by Japan Society for the Promotion of Science KAKENHI Grant 24K00795 to HS, 24K07171 and 23K25970 to KK, and 23H00152 to IK.

Declarations

Ethics declaration: Not applicable.

Conflict of interest: The authors declare no competing interests.

References

Barbot S (2024) Does the direct effect of friction increase continuously with absolute temperature? Proc Natl Acad Sci U S A 121:e2405111121. https://doi.org/10.1073/pnas.2405111121

Bedford JD, Faulkner DR (2021) The Role of Grain Size and Effective Normal Stress on Localization and the Frictional Stability of Simulated Quartz Gouge. Geophys Res Lett 48:e2020GL092023. https://doi.org/10.1029/2020GL092023

Bhattacharya P, Rubin AM, Bayart E, Savage HM, Marone C (2015) Critical evaluation of state evolution laws in rate and state friction: Fitting large velocity steps in simulated fault gouge with time-, slip-, and stress-dependent constitutive laws. J Geophys Res 120:6365–6385. https://doi.org/10.1002/2015JB012437

Brechet Y, Estrin Y (1994) The effect of strain rate sensitivity on dynamic friction of metals. Scr Metall Mater 30:1449–1454. https://doi.org/10.1016/0956-716X(94)90244-5

Chester FM, Higgs NG (1992) Multimechanism friction constitutive model for ultrafine quartz gouge at hypocentral conditions. J Geophys Res 97:1859–1870. https://doi.org/10.1029/91JB02349

Dieterich JH (1979) Modeling of rock friction: 1. Experimental results and constitutive equations. J Geophys Res 84:2161–2168. https://doi.org/10.1029/JB084iB05p02161

Dieterich JH, Conrad G (1984) Effect of humidity on time- and velocity-dependent friction in rocks. J Geophys Res 89:4196−4202. https://doi.org/10.1029/JB089iB06p04196

Heslot F, Baumberger T, Perrin B, Caroli B, Caroli C (1994) Creep, stick-slip, and dry-friction dynamics: Experiments and a heuristic model. Phys Rev E 49:4973–4988. https://doi.org/10.1103/PhysRevE.49.4973

Katayama I, Kubo T, Sakuma H, Kawai K (2015) Can clay minerals account for the behavior of non-asperity on the subducting plate interface? Prog Earth Planet Sci 2:30. https://doi.org/10.1186/s40645-015-0063-4

Kubo T, Katayama I (2015) Effect of temperature on the frictional behavior of smectite and illite. J Mineral Petrol Sci 110:293–299. https://doi.org/10.2465/jmps.150421

Leeman JR, Marone C, Saffer DM (2018) Frictional Mechanics of Slow Earthquakes. J Geophys Res 123:7931–7949. https://doi.org/10.1029/2018JB015768

Liu Y, He C (2023) Friction of hornblende and tremolite at hydrothermal conditions with low effective normal stress and high pore pressure. Tectonophysics 863:230002. https://doi.org/10.1016/j.tecto.2023.230002

Lloyd GE, Knipe RJ (1992) Deformation mechanisms accommodating faulting of quartzite under upper crustal conditions. J Struct Geol 14:127–143. https://doi.org/10.1016/0191-8141(92)90052-X

Masuda K, Arai T, Takahashi M (2019) Effects of frictional properties of quartz and feldspar in the crust on the depth extent of the seismogenic zone. Prog Earth Planet Sci 6:50. https://doi.org/10.1186/s40645-019-0299-5

329 Morrow CA, Moore DE, Lockner DA (2000) The effect of mineral bond strength and
330 adsorbed water on fault gouge frictional strength. Geophys Res Lett 27:815–818.
331 https://doi.org/10.1029/1999GL008401

332 Nakatani M (2001) Conceptual and physical clarification of rate and state friction: Frictional
333 sliding as a thermally activated rheology. J Geophys Res 106:13347–13380.
334 https://doi.org/10.1029/2000JB900453

335 Nakatani M, Scholz CH (2004) Frictional healing of quartz gouge under hydrothermal
336 conditions: 2. Quantitative interpretation with a physical model. J Geophys Res 109:
337 2003JB002938. https://doi.org/10.1029/2003JB002938

338 Niemeijer A, Marone C, Elsworth D (2010) Frictional strength and strain weakening in
339 simulated fault gouge: Competition between geometrical weakening and chemical
340 strengthening. J Geophys Res 115:2009JB000838. https://doi.org/10.1029/2009JB000838

341 Noda H, Shimamoto T (2009) Constitutive properties of clayey fault gouge from the Hanaore
342 fault zone, southwest Japan. J Geophys Res 114:2008JB005683.
343 https://doi.org/10.1029/2008JB005683

344 Rice JR, Lapusta N, Ranjith K (2001) Rate and state dependent friction and the stability of
345 sliding between elastically deformable solids. J Mech Phys Solids 49:1865–1898.
346 https://doi.org/10.1016/S0022-5096(01)00042-4

347 Ruina A (1983) Slip instability and state variable friction laws. J Geophys Res 88:10359–
348 10370. https://doi.org/10.1029/JB088iB12p10359

349 Sakuma H, Moore DE, Lockner DA, Kogure T (2026) Velocity-Independent Dry Friction
350 on Mica: Realization of Ideal Amontons-Coulomb Friction. Phys Rev Lett 137:046201.
351 https://doi.org/10.1103/y3jy-nqcd

352 Scholz CH (1998) Earthquakes and friction laws. Nature 391:37–42.
353 https://doi.org/10.1038/34097

354 Skarbek RM, Savage HM (2019) RSFit3000: A MATLAB GUI-based program for
355 determining rate and state frictional parameters from experimental data. Geosphere 15:1665–
356 1676. https://doi.org/10.1130/GES02122.1

357 Sleep NH (1997) Application of a unified rate and state friction theory to the mechanics of
358 fault zones with strain localization. J Geophys Res 102:2875–2895.
359 https://doi.org/10.1029/96JB03410

Supplementary Files

This is a list of supplementary files associated with this preprint. Click to download.

- Supplementarymaterial.docx